# NON-EQUILIBRIUM BED VARIATION ANALYSIS IN STONY-BED RIVERS CONSIDERING CHANGES IN THE BED SURFACE STRUCTURE: APPLICATION TO ENLARGEMENT MECHANISM OF THE MONOBE RIVER MOUTH DUE TO FLOODS

YOSHIHARU TAKEMURA
*Research and Development Initiative, Chuo University, Kasuga 1-13-27, Bunkyo-ku, Tokyo, Japan, E-mail: takemura@tamacc.chuo-u.ac.jp*

SHOJI FUKUOKA
*Research and Development Initiative, Chuo University, Kasuga 1-13-27, Bunkyo-ku, Tokyo, Japan, E-mail: sfuku@tamacc.chuo-u.ac.jp*

## ABSTRACT

The bar at the Monobe River mouth composed of gravel particles and cobbles narrows the width at the outlet to the sea. The second-largest flood occurred in July 2018 greatly enlarged the opening width of the river mouth and formed a spit-like depositional landforms at the coastal area. The sediment transport of gravel particles and cobbles are essentially non-equilibrium phenomena due to the influence of the unevenness of bed surface configurations and the local bed gradients. This paper proposes an analysis method that can demonstrate three-dimensional flood currents and non-equilibrium motion of gravel particles and cobbles by improving the bed variation analysis method for stony-bed rivers and combining it with the Q3D-FEBS. Moreover, it is shown that the proposed analysis method can explain the enlargement mechanism of the river mouth opening and the formation process of the depositional landforms at the coastal area than the conventional analysis method based on the equilibrium bed load formula.

*Keywords*: Flood flows, river mouth, Monobe River, Q3D-FEBS, non-equilibrium sediment transport

## 1. INTRODUCTION

Bars formed at a river mouth increase the risk of flood inundation and bank erosion by narrowing the passage of flood flows. River mouth bars are also related to the various problems such as intrusion of saltwater and waves into river channels, sediment supply in coastal zones, and fish migration. Therefore, it is necessary to explore the enlargement mechanism of a river mouth opening and the deposition process of the fluvial sediment at coastal areas during floods.

The bar composed of gravel particles and cobbles in the range 2–100 mm is formed in the Monobe River mouth. The gravel bar narrows the opening width of the river mouth as Figure 1 (a). The flood occurred in July 2018 is the second-largest flood in the history of the observation of the Monobe River. The July 2018 flood greatly enlarged the opening width of the river mouth and formed a spit-like depositional landforms at the coastal area (Figure 1 (b)).

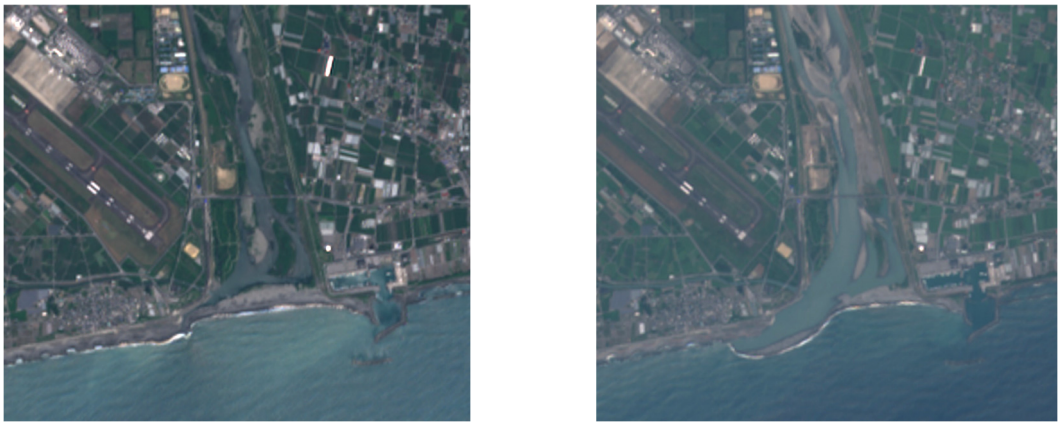

(a) 2018/6/13 10:47 (b) 2018/7/18 10:52

Figure 1. Satellite images of the Monobe River mouth (source: EO Browser).

Kadota et al. (2008) numerically investigate the enlargement mechanism of the Monobe River mouth opening by using the 3D flow model and the equilibrium bed load formula (Rijn, 1984). However, the Rijn's formula was proposed for sediment particles in the range 0.2-2.0 mm. The applicability to the Monobe river mouth is unknown. The transport mechanism of gravel particles and cobbles are essentially non-equilibrium phenomena because the threshold of sediment motion and transport process are largely affected by the unevenness of bed surface configurations (e.g., imbrication, cluster) and the local bed gradients.

Recently, we developed a new non-hydrostatic quasi three-dimensional model (Q3D-FEBS) that can calculate three-dimensional velocities and pressure distributions due to the complex riverbed topography with high computational efficiency compared to the 3D flow model (Takemura and Fukuoka, 2019). This paper proposes an analysis method that can demonstrate three-dimensional flood currents and non-equilibrium motion of gravel particles and cobbles by improving the bed variation analysis method for stony-bed rivers proposed by Osada and Fukuoka (2012) and combining it with the Q3D-FEBS. We analyze the enlargement mechanism of the river mouth opening and the formation process of the depositional landforms at the coastal area for the July 2018 flood in the Monobe River (see Figure 1(b)). Moreover, the importance of the non-equilibrium sediment motion to explain these phenomena was discussed from the comparison with the analysis results using the conventional bed variation analysis.

## 2. NUMERICAL ANALYSIS METHOD

### 2.1 Q3D-FEBS and the bed variation analysis method for stony-bed rivers (Osada and Fukuoka 2012)

The definition sketch of the Q3D-FEBS is shown in Figure 2. We define a bottom surface $z_b$ slightly above a mean bed surface $z_m$. A vertical coordinate is given as $\eta = (z_s - z)/h$ and approximates vertical distributions of the horizontal velocities by the third-order polynomial. In addition to the depth-average flow velocities, flow velocities at the free surface and bottom surface are solved by the equations of motion.

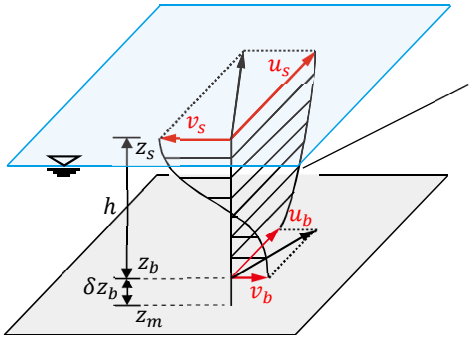


$$u_{xi} = (u_{s,x_i} - U_{x_i}) \cdot (12\eta^3 - 12\eta^2 + 1) + (u_{s,x_i} - u_{b,x_i}) \cdot (-4\eta^3 + 3\eta^2) + U_{x_i}$$

$$\eta = \frac{(z_s - z)}{h}$$

$u_{s,x_i}$: free surface velocities, $u_{b,x_i}$: bottom surface velocities
$U_{x_i}$: depth-average velocities, $h$: water depth
$z_s$: free surface, $z_b$: bottom surface, $z_m$: mean bed surface,
$\delta z_b$: distance between bottom surface and mean bed surface (= 0.03 $h$)

Figure 2. Definition sketch of the Q3D-FEBS.

The bed variation analysis method for stony-bed rivers (Osada and Fukuoka, 2012) is performed by non-equilibrium sediment motion by the continuity equation of bed load at non-equilibrium condition and the equation of motion for a sediment particle as follows.

$$\frac{\partial V_k}{\partial t} + \frac{\partial q_{bk,x_i}}{\partial x_i} = P_k - D_k \tag{1}$$

$$q_{bk,x_i} = \bar{u}_{pk,x_i} \cdot V_k \tag{2}$$

Where, $i = 1,2(x_1 = x, x_2 = y)$, $V_k$: bed load volume of particles of size $d_k$ per unit area, $q_{bk,xi}$: bed load rate of particles of size $d_k$ per unit width in $x_i$ direction, $\bar{u}_{pk,xi}$: mean velocity of particles of size $d_k$ in $x_i$ direction, $P_k$: pick up rate of particles of size $d_k$ per unit area, $D_k$: deposition rate of particles of size $d_k$ per unit area.

$$(\rho_s + \rho C_m)\alpha_3 d_k^3 \frac{du_{pk,x_i}}{dt} = \rho_s \alpha_3 d_k^3 \boldsymbol{g}_{\boldsymbol{x_i}} - \alpha_3 d_k^3 \left(\rho g \frac{\partial z_s}{\partial x_i} + \frac{\partial p_b'}{\partial x_i}\right) + \frac{\rho C_D \alpha_2 d_k^2}{2} u_{rk,x_i} \sqrt{u_{rk,x_j}^2} \tag{3}$$

Where, $i = 1,2,3(x_1 = x, x_2 = y, x_3 = z)$, $\boldsymbol{g}_{\boldsymbol{x_i}} = (0,0,-g)$, $g$: acceleration of gravity, $\rho$: density of water, $\rho_s$: density of sediment, $u_{pk,xi}$: velocity of particles of size $d_k$ in $x_i$ direction, $u_{rk,x_i}$:relative velocity between fluid and particles of size $d_k$ in $x_i$ direction, $p_b'$: non-hydrostatic pressure at the bottom surface, $C_D$: drag coefficient (= 0.4), $C_m$: added mass coefficient (= 0.5), $\alpha_2$, $\alpha_3$:2D and 3D shape factor of particles (= $\pi/4$, $\pi/6$). The pressure gradients in Eq. (3) are evaluated from the Q3D-FEBS. $\bar{u}_{pk,xi}$ shown in Eq. (2) are calculated from the saltation analysis using Eq. (3). $P_k$ and $D_k$ are calculated by considering the height distribution of stationary particles in a bed surface layer in order to incorporate the effects of the unevenness of bed surface configurations in stony-bed rivers. The height distribution of the particles is calculated by the following manner. ①: Calculate

the mean height of the centroid of particles of each size in a bed surface layer $\bar{z}_k$. ②: Assume that the height of the centroid of particles of each size is normally distributed around $\bar{z}_k$ as Figure 3.

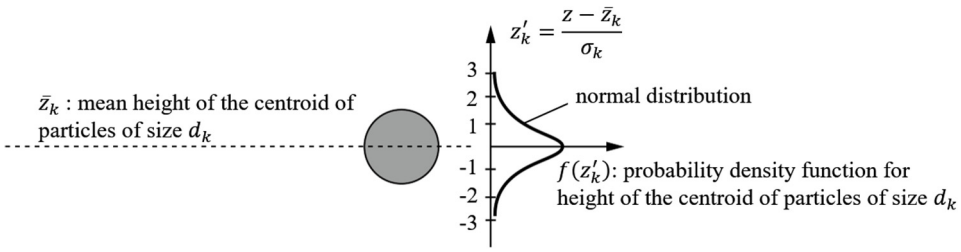


Figure 3. Height distribution of each particle.

However, the calculation method of $\bar{z}_k$ proposed by Osada and Fukuoka (2012) has a problem that the change in volume fraction of each particle in a bed surface layer is neglected. The paper corrects this problem and proposes the new calculation method of $\bar{z}_k$. Moreover, based on this correction, the threshold for the sediment motion and the pickup rate of nonuniform sediment are reformulated.

## 2.2 Calculation method of the average height of each particle

We define the bed surface layer and subsurface layer as Figure 4.

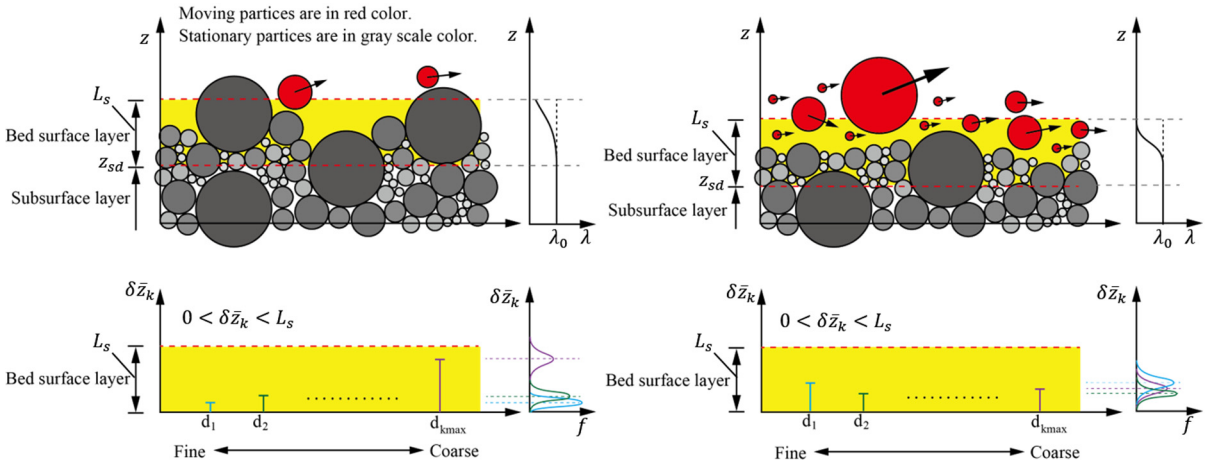


(1) Coarse particles hardly move. (2) Coarse particles move actively.

Figure 4. Definition sketch of a bed surface layer and a subsurface layer.

The subsurface layer is defined as a layer in which the porosity of sediment can be regarded as substantially constant. The bed surface layer is defined as a layer above the subsurface layer in which the stationary particles can exist on average. $z_{sd}$ is the elevation of the interface of the bed surface layer and the subsurface layer. The average height of the centroid of the stationary particle of size $d_k$ relative to $z_{sd}$ in the bed surface layer can be defined as

$$\delta\bar{z}_k = \frac{1}{n_k}\sum_{n_k}(z_k - z_{sd}) \tag{4}$$

where, $n_k$: number of the stationary particles of size $d_k$ in the bed surface layer, $z_k$: height of the centroid of particles of size $d_k$. Thus, the temporal changes in $\delta\bar{z}_k$ can be written as

$$\frac{\partial\delta\bar{z}_k}{\partial t} = -\frac{\delta\bar{z}_k}{n_k}\frac{\partial n_k}{\partial t} + \frac{1}{n_k}\sum_{n_k}\frac{\partial z_k}{\partial t} - \frac{\partial z_{sd}}{\partial t} \tag{5}$$

The second term of the right-hand side of Eq. (5) can be written as

$$\frac{1}{n_k}\sum_{n_k}\frac{\partial z_k}{\partial t} = -\frac{\alpha_2}{\alpha_3}\frac{(P_k - D_k)}{p_k} \tag{6}$$

where, $p_k$: volume fraction of the stationary particle of size $d_k$ in the bed surface layer. $n_k$ is expressed by using the volume of the stationary particles of size $d_k$ in the bed surface layer $V_s$ and $p_k$ as $V_s \cdot p_k/(\alpha_3 d_k^3)$. We can obtain Eq. (7) from Eq. (5) by assuming $V_s$ has a constant value.

$$\frac{\partial\delta\bar{z}_k}{\partial t} = -\frac{\delta\bar{z}_k}{p_k}\frac{\partial p_k}{\partial t} - \frac{\alpha_2}{\alpha_3}\frac{(P_k - D_k)}{p_k} - \frac{\partial z_{sd}}{\partial t} \tag{7}$$

The temporal changes in $z_{sd}$ and $p_k$ are calculated by

$$\frac{\partial z_{sd}}{\partial t} = -\sum_{k_{max}} \frac{\alpha_2}{\alpha_3}(P_k - D_k) \tag{8}$$

$$\frac{\partial p_k}{\partial t} = -\frac{1}{L_s}\frac{\alpha_2}{\alpha_3}(P_k - D_k) - \frac{p_k|_{z_{sd}}}{L_s}\frac{\partial z_{sd}}{\partial t} \qquad \frac{\partial z_{sd}}{\partial t} \geq 0 \quad p_k|_{z_{sd}} = p_k \quad \frac{\partial z_{sd}}{\partial t} < 0 \quad p_k|_{z_{sd}} = p_{k0} \tag{9}$$

where, $k_{max}$: number of different particle sizes, $p_{k0}$:volume fraction of particles of size $d_k$ in the subsurface layer, $L_s$: thickness of the bed surface layer. Substituting Eq. (8) and Eq. (9) into Eq. (7), the temporal changes in $\delta\bar{z}_k$ is calculated by

$$\frac{\partial \delta\bar{z}_k}{\partial t} = -\left(1 - \frac{\delta\bar{z}_k}{L_s}\right)\frac{\alpha_2}{\alpha_3}\frac{(P_k - D_k)}{p_k} + \left(1 - \frac{\delta\bar{z}_k}{L_s}\frac{p_k|_{z_{sd}}}{p_k}\right)\sum_{k_{max}}\frac{\alpha_2}{\alpha_3}(P_k - D_k) \tag{10}$$

The first term of the right-hand side of Eq. (10) represents the effects of sediment exchange with the bed load and the second term represent the effects of sediment exchange with the subsurface layer.

The height distributions of the centroid of particles of size $d_k$ are given as

$$f(z_k') = \frac{1}{\sqrt{2\pi}} exp\left(-\frac{{z_k'}^2}{2}\right), z_k' = \frac{z - \bar{z}_k}{\sigma_k} \tag{11}$$

$$\sigma_k = min(\delta\bar{z}_k, 0.5L_s) \cdot min\left\{0.435 + exp\left(-6\frac{d_k}{d_m}\right), 0.6\right\} \tag{12}$$

where, $f(z_k')$: probability density function for the height of the centroid of particles of size $d_k$, $d_m$: mean diameter of the stationary particles in the bed surface layer.

## 2.3 Threshold for the sediment motion and the pickup rate for nonuniform sediment

The pickup rate of particles of size $d_k$ in the bed surface layer is calculated by Eq. (14).

$$P_k = \varepsilon_p\left(\frac{p_k}{\alpha_2 d_k^2}\right)\left(\frac{\alpha_3 d_k^3}{T_{pk}}\right) \tag{14}$$

Where, $\varepsilon_p$: volume fraction of the stationary particles of size $d_k$ in the bed surface layer that start to move, $T_{pk}$: time required for the stationary particles of size $d_k$ in the bed surface layer to be entrained into the bed load. The stationary particle at a height of $z_k' = 2.2\sigma_k$ (see Figure 3) are used for determining the threshold of sediment motion. Assume that if the fluid dynamic forces acting on the particle exceed the threshold, the particles existing above $z_k' = 2.2\sigma_k$ are entrained into the bed load. Then the value of $\varepsilon_p$ can be obtained as 0.014 from Eq. (11). The fluid dynamic forces acting on the particle are assumed as Figure 5.

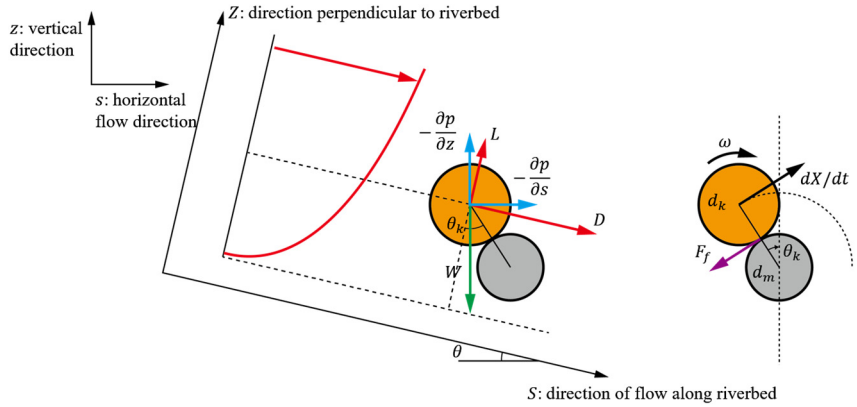


Figure 5. Fluid dynamic forces acting on a particle.

Driving the equation for rotation angle $\theta_k$ according to Nakagawa et al. (1991) as

$$\frac{d^2\theta_k}{dt^2} = \frac{-W'sin\theta_k + F_s cos\theta_k + F_z sin\theta_k}{(\rho_s + \rho C_m)\alpha_3 d_k^3 \frac{7}{10}(d_m + d_k)} \tag{15}$$

$$F_S = \varepsilon\,\rho\frac{1}{2}C_D\alpha_2 d_k^2 u_f^2 + \left(-\rho g\frac{\partial z_s}{\partial s} - \frac{\partial p'}{\partial s}\right)\alpha_3 d_k^3 cos\theta - \left(\rho g - \frac{\partial p'}{\partial z}\right)\alpha_3 d_k^3 sin\theta \tag{16}$$

$$F_Z = \varepsilon\,\rho\frac{1}{2}C_L\alpha_2 d_k^2 u_f^2 + \left(\rho g - \frac{\partial p'}{\partial z}\right)\alpha_3 d_k^3 cos\theta + \left(-\rho g\frac{\partial z_s}{\partial s} - \frac{\partial p'}{\partial s}\right)\alpha_3 d_k^3 sin\theta \tag{17}$$

$$\frac{u_f}{u_*} = \frac{1}{\kappa} log\left(30.2\frac{z_{pt} - z_{sd}}{d_r}\right) \tag{18}$$

where, $W' = \rho_s\alpha_3 d_k^3 cos\theta$, $z_{pt}$: height of particles at $z_k' = 2.2\sigma_k$ in the bed surface layer. $\varepsilon$: shielding coefficient (= 0.4), $C_D$: drag coefficient (= 0.4), $C_L$: lift coefficient (= 0.4), $d_r$: representative diameter of sediment particles in the bed surface layer. The pressure gradients including Eq. (16) and Eq. (17) are evaluated from Q3D-FEBS.

$T_{pk}$ can be calculated by solving Eq. (15) numerically until the $\theta_k$ becomes 0 under the conditions that $\theta_k = -\theta_{k0}$ and $d\theta_k/dt = 0$ at $t = 0$. However, we use the theoretical solution for the simplicity and computational efficiency. Eq. (19) can be obtained by assuming the fluid dynamic forces acting on the particle unchanged until the particle entrained into the bed load.

$$T_{p_k} = \sqrt{2\theta_{k0}/A} \tag{19}$$

$$A = \frac{-W'sin\theta_{k0} + F_s cos\theta_{k0} + F_z sin\theta_{k0}}{(\rho_s + \rho C_m)\alpha_3 d_k^3 \frac{7}{10}(d_m + d_k)} \tag{20}$$

$$\theta_{k0} = \cos^{-1}\left[\frac{0.32d_m + 0.5d_k}{0.5(d_m + d_k)}\right] \tag{21}$$

The threshold for sediment motion of each particle size can be investigated by putting the left-hand side of the Eq. (20) as 0 ($A$ = 0). Figure 6 shows an example of the relationship between the dimensionless critical shear stress $\tau_{*ck}$ ($= \rho u_*^2/((\rho_s - \rho)gd_k)$) and the particle size ratio $d_k/d_m$, and $\delta\bar{z}_k$ (mean height of the particle of size $d_k$ relative to $z_{sd}$ in the surface layer). $d_m$ is the mean diameter of the particles in the surface layer and $u_*$ is the bed shear velocity. The thickness of the surface layer $L_s$ is given by the representative diameter $d_r$. Therefore, $\delta\bar{z}_k/d_r$ (or $\delta\bar{z}_k/L_s$) has a value between 0 to 1 for each particle size. $\tau_{*ck}$ decreases as the values of $d_k/d_m$ and $\delta\bar{z}_k/d_r$ increases, and vise vasa. In the stony bed river, the fine particles can be hidden at the lower part of the bed surface layer in the situation that the coarse particles can stay on the upper part of the bed surface layer (see Figure 4 (a)). Contrary, fine particles are exposed on the upper part of the bed surface layer and easily entrained into the flows when coarse particles actively move (see Figure 4 (b)). Such mechanisms are important to analyze the bed variations in the stony-bed rivers, but it will be difficult to explain from the conventional methods in which $\tau_{*ck}$ has a specific value against the particle size ratio such as $d_k/d_m$. Our method can determine $\tau_{*ck}$ by considering the relative height of each particle in the bed surface layer in addition to the particle size ratio as shown in Figure 6. Therefore, it is more suitable for the bed variation analysis in the stony-bed rivers than the conventional methods.

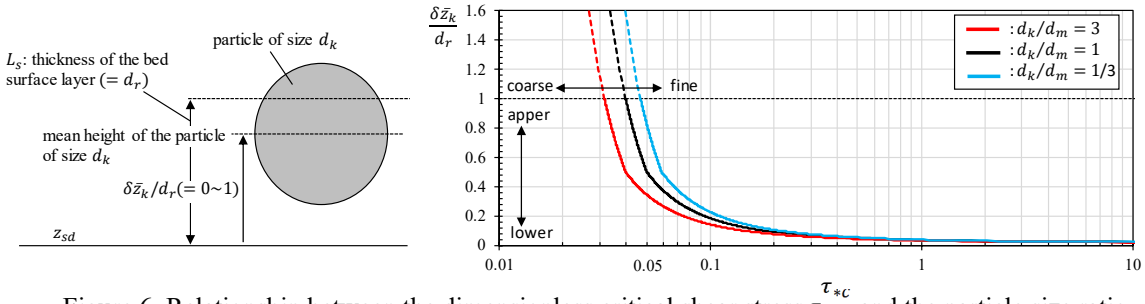


Figure 6. Relationship between the dimensionless critical shear stress $\tau_{*ck}$ and the particle size ratio, and the average height of particles relative to $z_{sd}$ in the bed surface layer $\delta\bar{z}_k$.

## 3. ENLARGEMENT MECHANISM OF RIVER MOUTH BAR IN THE MONOBE RIVER DUE TO THE JULY 2018 FLOOD

### 3.1 The July 2018 flood and the observation system of the studied reach

The Monobe River is in the Kochi Prefecture, Japan. Figure 7 shows the observation system of the studied reach. Pressure type water level gauges have been installed at the point of 🔴.

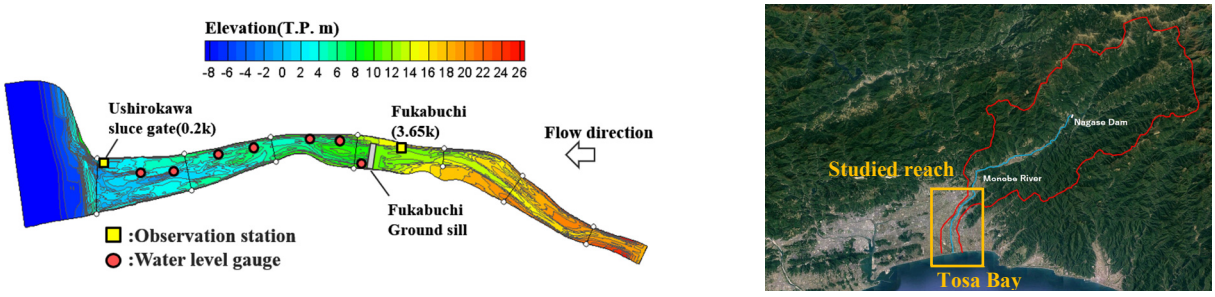


Figure 7. Observation system at the studied reach.

Figure 8 shows the observed discharge hydrograph at Hukabuchi (3.65km), sea level and significant wave height at the Tosa Bay during the July 2018 flood. The opening width of the river mouth was greatly enlarged, and a spit-like depositional landforms were formed in the coastal area during the flood as shown in Figure 1. The flood water surface profiles were observed by the water level gauges installed at the location shown in Figure 7. Besides, bed topography around the river mouth was measured just after the flood (see Figure 8).

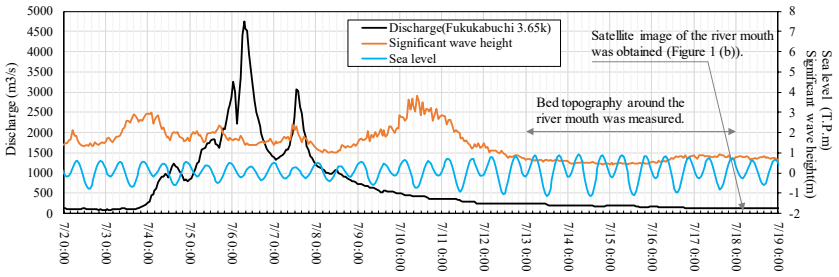


Figure 8. Observed discharge hydrograph at Hukabuchi (3.65km), sea level and significant wave height at the Tosa Bay during the flood in July 2018.

## 3.2 Computational conditions

The boundary conditions at the upstream and downstream ends are given by the observed water level hydrographs at Fukabuchi (3.65 km) and the sea level hydrograph, respectively. Figure 9 shows the particle size distributions of sediment material used for the bed variation analysis. The maximum diameter of the sediment particle is 150 mm. The particle size distributions of the river channel and the gravel bar at the river mouth are determined based on the measurement, respectively. We determine the $d_{90}$ as the representative diameter $d_r$ and the thickness of the bed surface layer $L_s$. $\varepsilon_p$ shown in Eq. (14) is determined as 0.018. Further study is needed for the value of $\varepsilon_p$.

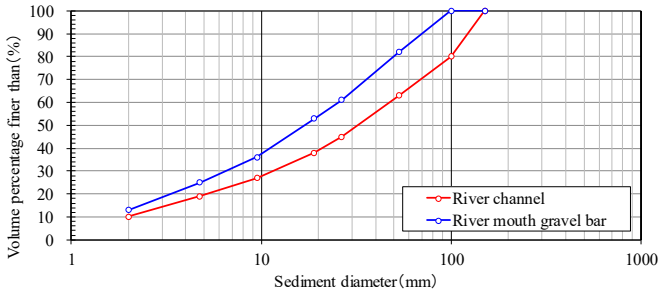


Figure 9. Particle size distributions of sediment material used for the bed variation analysis.

## 3.3 Enlargement mechanism and deposition process at the coastal area during the July 2018 flood

Figure 10 shows the comparison of the observed and the calculated water surface profiles in the rising period of the July 2018 flood.

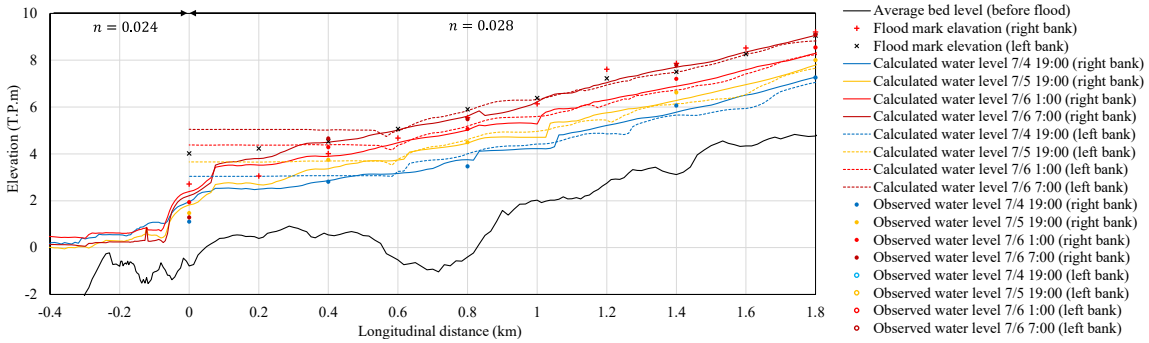


Figure 10. Comparison of observed and calculated water surface profiles in the rising period of the July 2018 flood.

The calculated water surface profiles can almost explain the observed water surface profiles and flood mark profile. The difference of the water levels between the left bank and right bank becomes extremely large due to the flood flow concentrated near the right bank around the river mouth. Figure 11 shows the comparison of the observed and the calculated discharge hydrographs at the Fukabuchi (3.65km) in the July 2018 flood. The calculation results show good agreement with the observation results.

Figure 12 shows the comparison of the observed and calculated bed topography around the river mouth after the July 2018 flood. The calculation results are shown in two cases. Figure 12 (c) is the result using the analysis method proposed by this paper (proposed model) and Figure 12 (d) is the result using the Ashida-Michiue formula (1972) that is the equilibrium bed load formula commonly used in Japan (conventional model). As shown in Figure 12 (a) and Figure 12 (b), the opening width of the river mouth at -0.2km point is enlarged about 480m and a spit-like depositional landforms are formed. The proposed model (Figure 12 (c)) shows that the opening width is slightly smaller and the deposition height of the fluvial sediments at the coastal area is lower than the observation results (Figure 12 (b)). However, the proposed model shows the promising result in the opening width of the river mouth and the depositional landforms at the coastal area than the conventional model.

Total amount of the sediment discharged from the river mouth to the coastal area estimated from the proposed model is 58764m$^3$.

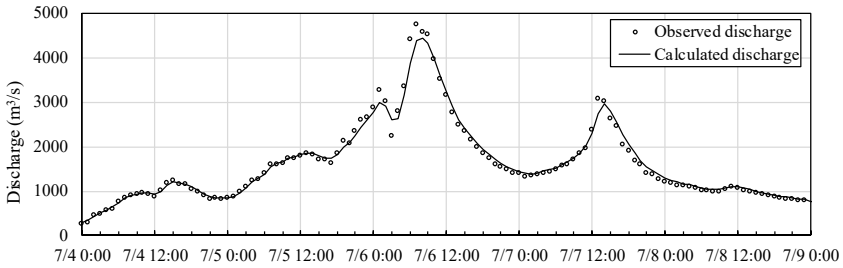


Figure 11. Comparison of observed and calculated discharge hydrograph at the Fukabuchi (3.65 km) in the July 2018 flood.

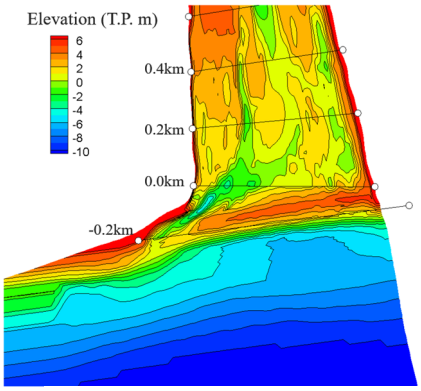


(a) Before the July 2018 flood.

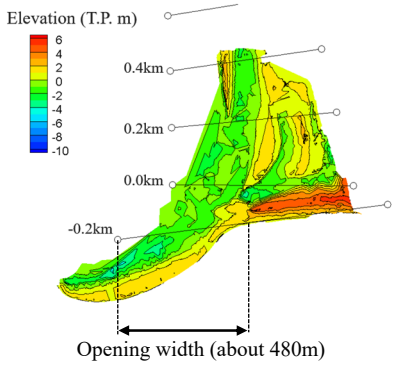


(b) After the July 2018 flood (observation).

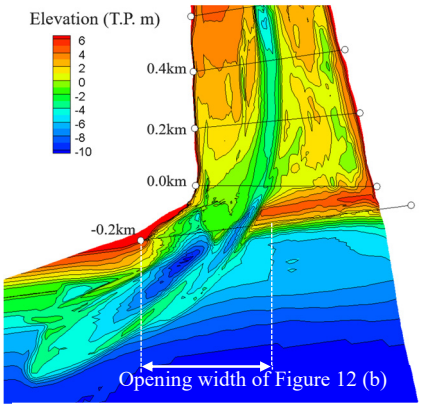


(c) After the July 2018 flood (calculation of the proposed model).

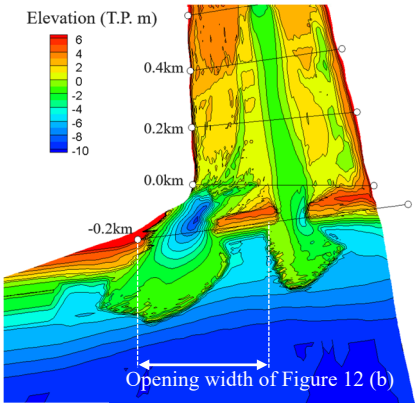


(d) After the July 2018 flood (calculation of the conventional model)

Figure 12. Comparison of the observed and calculated bed topography around the river mouth after the July 2018 flood.

In the followings, we investigate the flood flows and sediment transport mechanisms around the river mouth based on the calculation results of the proposed model. Figure 13 shows the water surface velocities and bottom surface velocities around the river mouth opening and the velocity distributions in -1.0km and -2.0km cross-sections at the peak of the July 2018 flood. The flood flows passing through the river mouth opening are greatly accelerating in the longitudinal direction and high velocity zones are found near the gravel bar as seen in Figure 13 (b). In addition, a strong secondary current is formed at upstream of the gravel bar.

Figure 14 shows the trajectories of the sediment particles of 100 mm and 2mm and the longitudinal distributions of the bed load around the river mouth opening at the peak of the July 2018 flood. As shown in Figure 14 (a), the motion of the coarse particles (100mm) is affected by local riverbed gradients compared to the fine particles (2mm). The motion of the coarse particles on the gravel bar (see circle I in Figure 14 (a)) accelerates the enlargement of the opening width of the river mouth. On the other hand, the coarse particle cannot easily cross the sediment deposited at the coastal area (see circle Ⅱ in Figure 14 (a)). This is considered to be one of the reasons that the spit-like depositional landforms were formed at the coastal area (Figure 12 (b)). As shown in Figure 14 (b) and (c), the bed load increases sharply from the downstream of 0.0km point due to the influence of the highly nonuniform flood flows as mentioned by Figure 13. The total bed load is the same order as the conventional model, but the longitudinal distribution is significantly different. From the above considerations, the sediment transport in the Monobe River mouth is largely affected by the three-dimensional currents and the local riverbed gradients. Therefore, the non-equilibrium motion of the sediment particles plays an important

role for the enlargement of the river mouth opening and the deposition process of the fluvial sediment at the coastal area.

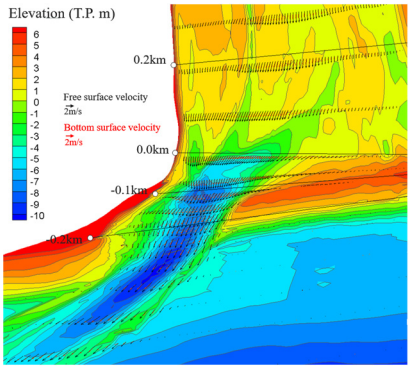


(a) Free surface and bottom surface velocities.

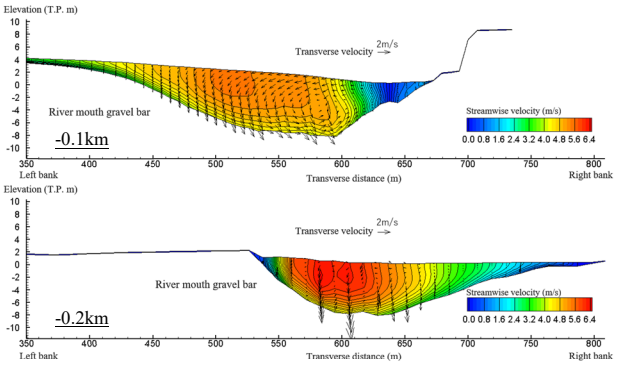


(b) Velocity distributions in -0.1 and -0.2 km cross-sections.

Figure 13. Calculated water surface velocities and bottom surface velocities around the river mouth opening and velocity distributions at -0.1 and -0.2 km cross-sections at the peak of the July 2018 flood.

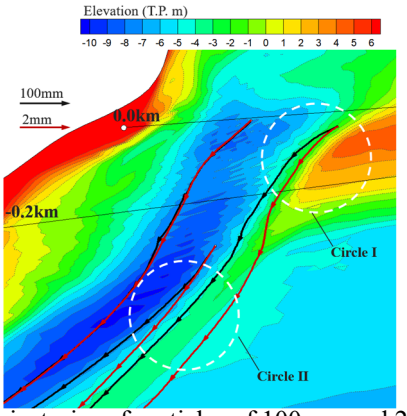


(a) Trajectories of particles of 100mm and 2mm.

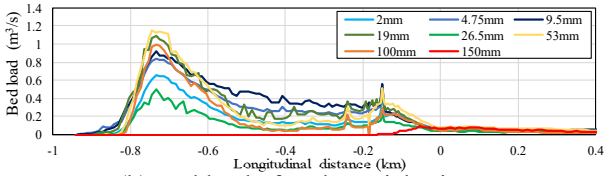


(b) Bed load of each particle size.

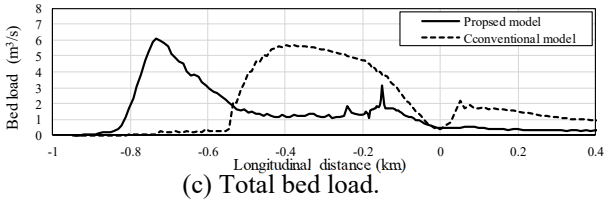


(c) Total bed load.

Figure 14. Calculated free surface velocities and bottom surface velocities around the river mouth opening and velocity distributions at -0.1 and -0.2 km cross-sections at the peak of the July 2018 flood.

## 4. CONCLUSIONS

This paper proposed an analysis method that can demonstrate the three-dimensional flood currents and non-equilibrium motion of the gravel particles and cobbles by improving the bed variation analysis method for the stony-bed rivers (Osada and Fukuoka, 2012) and combining it with the Q3D-FEBS.

The proposed analysis method was able to explain the enlargement mechanism of the river mouth opening and the formation process of the depositional landforms at the coastal area for the July 2018 flood in the Monobe River than the conventional analysis method based on the equilibrium bed load formula. However, the proposed analysis method showed that the opening width was slightly smaller and the deposition height of the fluvial sediment at the coastal area was lower than the observation results.

## REFERENCES


Ashida, K. and Michiue, M. (1972). Study on hydraulic resistance and bed-load transport rate in alluvial streams, Transactions, Journal of Japan Society of Civil Engineers, Vol.208, pp.59-69 (in Japanese).

Osada, K. and Fukuoka, S. (2012). Two-dimensional riverbed variation analysis method focused on the mechanism of sediment transport and the bed surface unevenness in stony-bed rivers, Journal of Japan Society of Civil Engineers, Ser. B1 (Hydraulic Engineering), Vol.68, No.1, pp.1-20 (in Japanese).

Kadota, A., Ishimoto, C., Nakano, S. and Szuki, K. (2008). Analyses for causes of river mouth blockade and formation/destraction of sand bar at Monobe River, Annual Journal of Hydraulics Engineering, JSCE, Vol.52, pp.601-606 (in Japanese).

Takemura, Y. and Fukuoka, S. (2019). Analysis of the flow in undular and hydraulic jump stilling basins using non-hydrostatic quasi-three dimensional model considering flow equations on boundary surfaces, Journal of Japan Society of Civil Engineers, Ser. B1 (Hydraulic Engineering), Vol.75, No.1, pp.61-80 (in Japanese).

Rijn, L.C. van (1984). Sediment transport, PartI: Bed load transport, Journal of Hydraulic Engineering, ASCE, Vol.110, No.10, pp.1431-1456.

Nakagawa, H., Tsujimoto, T. and Gotoh, H. (1991). Dislodgement process of sediment particles on bed at unsteady flow, Rijn, L.C. van (1984). Sediment transport, Annual Journal of Hydraulics Engineering, JSCE, Vol.35, pp.429-434 (in Japanese).